Classification of Multi-layer Tissue-mimicking Dielectric Stacks from 2 GHz to 20 GHz

Robert Streeter, *Member, IEEE*, Jooeun Lee, *Graduate Student Member, IEEE*, Gabriel Santamaria Botello, *Member, IEEE*, Zoya Popović, *Fellow, IEEE*

***Abstract*—Determination of the thickness, permittivity, and conductivity of tissue layers in the microwave region of the electromagnetic spectrum is relevant to a number of applications, such as breast-cancer imaging and non-invasive subcutaneous tissue thermometry. Many current characterization approaches are limited to one or two layers, often required to be aqueous. This paper presents simplified modeling of a stack of tissue layers as a series of complex impedance transmission lines in the 2 – 20 GHz decade. A near-field, broadband interrogation antenna designed for this frequency range and placed on the skin is validated with complex reflection coefficient measurements on seventeen different stacks of materials. Initial measurements are used to build a lookup table of features that are then used to classify three independent sets of follow-up measurements on the same stacks. After processing and consideration of very thin and very low loss materials, the error rates for classification are found to be between 5.9% and 14.7%. This confirms that features extracted from a simple, calibrated one-port broadband reflection coefficient measurement provide sufficient information to identify the composition of a layered stack, modeling tissue layers.**

***Index Terms*—dielectric measurement, microwave radiometry**

I. Introduction

CHARACTERIZING the properties of a stack of lossy, planar, dielectric layers, such as human tissues, is a topic of interest. Not only does *in vivo* characterization of tissues offer stand-alone diagnostic potential, for instance in measuring hydration [1] or impacts of hyperthermia therapy [2], it also provides crucial information for tissue stack modeling, which is needed, e.g., for wearable sensors including microwave thermometry [3], [4] or glucose monitoring [5]. Current techniques for measuring the electromagnetic (EM) properties of a sample (i.e., permittivity ϵ_r and conductivity σ) include open-ended coaxial probes [6], [7], various resonators such as parallel plates [8] or microstrip [9], among others. In general all these techniques are limited to only one or two layers and in the case of the resonators, require the sample to be excised prior to measurement.

Here, we demonstrate a technique for characterizing both the EM properties and layer thicknesses of a multi-layered stack of lossy dielectrics as illustrated in Fig.1. A broadband interrogation near-field antenna (NFA) is placed directly against the stack. Connected to the antenna is a calibrated VNA, which is used to take a one-port reflection coefficient measurement. Data from this complex measurement are imported into MATLAB and either added to a lookup table or compared to an existing lookup table for classification. The resulting knowledge of tissue properties allows computation of the near-field sensitivity region [10], which is necessary for accurate microwave thermometry measurements of deep tissue layers. For example, physiologically reasonable changes in tissue thicknesses of the forehead, based on the literature [11], can result in changes to measured temperature of the brain. Tissue thickness is also important for microwave breast imaging and cancer detection [12] as well as during hyperthermia therapy [2].

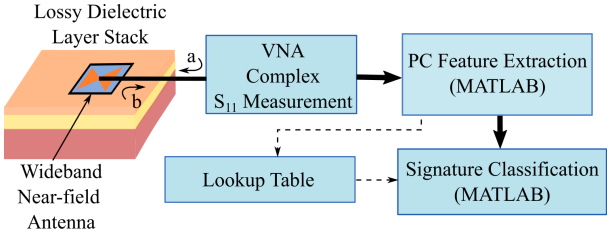

Fig. 1. High-level block diagram of the measurement system for tissue characterization. An interrogation antenna is placed on a stack to be measured. Then, a calibrated single-port complex reflection coefficient measurement is made using a vector network analyzer. The incident wave from the analyzer is 'a,' and corresponding reflected wave is 'b.' The complex reflection coefficient, $\frac{b}{a}$, is measured. This data is then processed, either to become part of a lookup table or compared to a lookup table for classification.

This paper is organized as follows. In Sec.II a stack of tissue layers is modeled as cascaded transmission lines with complex characteristic impedances and complex propagation coefficients. This model can be used to determine a stack's unique "signature" in the frequency domain. Next, the design of a broadband, NFA is detailed in Sec.III. Lastly, in Sec.IV, measurements using this antenna against a number of stack configurations are provided and the viability of this approach is illustrated. Conclusions and avenues for future work are mentioned in Sec.VI.

II. Transmission Line Approximation

During the VNA measurement, a sweep of time-harmonic waves in the microwave region of the EM spectrum are emitted into the stack under test. These signals are represented by the

This work was supported by NSF grant 2026523 and a Lockheed Martin Endowed Chair.

Robert Streeter is with LumenAstra, 12416 N 63rd St, Longmont, CO 80503.

Jooeun Lee and Zoya Popović is with the Univ. of Colorado at Boulder, 425 UCB, Boulder, CO 80309.

Gabriel Santamaria Botello is with the Colorado School of Mines, 1500 Illinois St, Golden, CO 80401.

Correspondence: Dr. Streeter (e-mail: rost3519@colorado.edu).

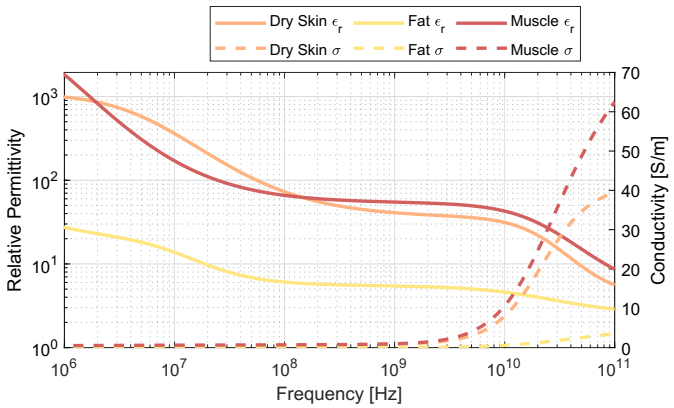

Fig. 2. Dispersive tissue properties of skin, fat, and muscle. Gabriel et al. utilized the Cole-Cole curve-fitting model to fit measurements of these tissues in their 1996 work [13].

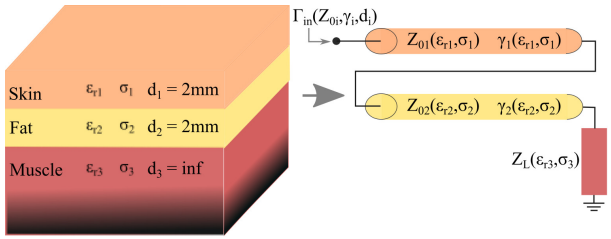

Fig. 3. Modeling a stack of layers as a cascade of complex impedance transmission lines. The permittivity, ϵ_r, and conductivity, σ, of each layer are mapped into the complex characteristic impedance, Z_0, and complex propagation coefficient, γ, of each line segment of length d_i. The muscle is treated as being infinitely thick and is thus a complex load at the end of the line cascade.

'a' waves in Fig.1, with corresponding reflected waves shown as 'b' waves. The resulting near field under the NFA in a multi-layer stack of dispersive, lossy tissues is complicated, and modeling is required to inform design of the NFA. To reduce complexity and simulation time, a stack of skin, fat, and muscle, with dispersive properties shown in Fig. 2, is modeled as a cascade of transmission lines with complex characteristic impedances. This models a single plane-wave at normal incidence from a transmitting antenna in the far field, at each frequency in the sweep.

Fig. 3 illustrates how the properties of a stack of three layers are mapped to the complex characteristic impedance, Z_{0i}, and complex propagation coefficient, γ_i, of a cascaded set of transmission lines. The innermost muscle layer is assumed to be sufficiently thick so as to appear infinite and thus represented as a complex load, Z_L. First, the characteristic impedance of each layer is computed as

$$Z_{0i} = \sqrt{\frac{j\omega\mu_0}{\sigma_i + j\omega\epsilon_0\epsilon_{ri}}}, \tag{1}$$

where $\omega = 2\pi f$ is the angular frequency, μ_0 and ϵ_0 the permeability and permittivity of free-space, respectively (the materials considered here are assumed sufficiently non-magnetic that $\mu_r = 1$), and σ_i and ϵ_{ri} are the conductivity (in S/m) and relative permittivity of layer i accordingly. Next, the complex propagation coefficient, γ_i, for each layer can be determined using

$$\gamma_i = \alpha + j\beta = j\omega\sqrt{\mu_0\epsilon_0\epsilon_{ri}}\sqrt{1 - j\frac{\sigma_i}{\omega\epsilon_0\epsilon_{ri}}}. \tag{2}$$

The equivalent input impedance can then be recursively computed for each layer using

$$Z_{in,i} = Z_{0i}\frac{Z_{in,i+1} + Z_{0i}\tanh(\gamma_i d_i)}{Z_{0i} + Z_{in,i+1}\tanh(\gamma_i d_i)}, \tag{3}$$

where Z_{0i} is the characteristic impedance of the current layer, $Z_{in,i+1}$ is the equivalent input impedance of all the layers below the current layer, and γ_i and d_i are the complex propagation constant and thickness of the current layer, respectively. For the innermost layer, $Z_{in,N} = Z_{0,N}$, where $N = 3$ in Fig. 3. Layers are then considered in sequence until the outermost layer is reached, resulting in an equivalent input impedance of the entire stack. The resulting input reflection coefficient, Γ_{in} can then be computed from

$$\Gamma_{in} = \frac{Z_{in,2} - Z_{01}}{Z_{in,2} + Z_{01}}e^{-2\gamma_1 d_1}, \tag{4}$$

which is the reflection coefficient at the boundary between the first and second outer layers (the skin and fat in this case), phase shifted across the outermost layer. It is important to bear in mind that the input impedance is generally complex and thus Eqn. (4) represents a complex ratio with an additional phase term. Furthermore, this assumes a frequency independent interrogation antenna that is perfectly matched to the skin layer.

This Γ_{in} is referred to as the "frequency domain signature." For the three-layer stack of in Fig. 3, the above approach, implemented in MATLAB, produces the complex signature shown in Fig. 4, with both magnitude as well as real and imaginary components plotted. Of note is the shaded region from about 2 GHz to 20 GHz. Within that range, as the component plots illustrate, there are high derivatives with respect to frequency. These rapid changes in the real and imaginary components of Γ_{in} suggest meaningful information may be extracted from that range. In this figure, the complex characteristic impedance of just the deeply buried muscle layer, represented by a complex load, is swept $\pm 10\%$ from nominal. This simulation illustrates that changes in tissue properties can be expected to produce corresponding changes in the reflection coefficient measured at the outermost layer. Therefore, this approach is pursued and 2 GHz to 20 GHz is selected as the frequency range of interest for the remainder of this paper.

III. Interrogation Antenna Design

In order to perform measurements of assembled layer stacks, a broadband, planar near-field interrogation antenna is designed through simulation in Ansys HFSS from 1 GHz to 20 GHz. A bow-tie architecture is selected as it is simple and fast to manufacture as well as sufficiently broadband. A schematic of the interrogation antenna is shown in Fig. 5, with simulated surface current magnitude plotted on the metalization. As expected, the current maintains a similar shape across

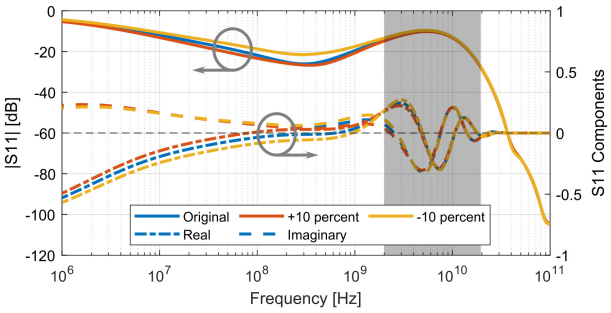

Fig. 4. The frequency domain signature of a three-layer stack of skin, fat, and muscle modeled as a cascade of transmission lines. The shaded region from about 2 GHz to 20 GHz contains rapidly changing complex components and is thus identified as the region of interest. The complex characteristic impedance of the deepest layer is swept ±10% from nominal. This illustrates that changes in deeply buried layer properties result in representative shifts in simulated Γ_{in}.

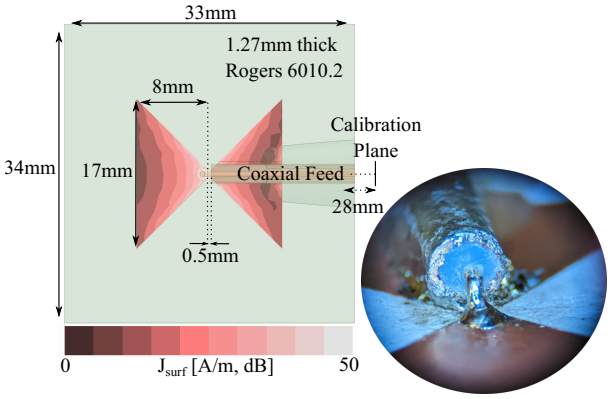

Fig. 5. Near-field interrogation antenna manufactured on Rogers 6010.2 ($\epsilon_r \approx 12.3$). The simulated total surface current magnitude, J_{surf}, is shown at 1 GHz. During measurement, the VNA is calibrated to the connector of the NFA, which is 28 mm from the edge of the substrate. Inset at bottom right is a photograph of the assembled feed point in the center of the NFA.

the frequency range and is concentrated closer to the feed point at higher frequencies. For all measurements, the calibration plane is the connector at the end of the coaxial feed of this NFA, which is 28 mm from the edge of 1.27 mm thick Rogers 6010.2 substrate. A photograph of the assembled antenna feedpoint is inset in the figure. The coaxial line diameter is about 2.3 mm. Measurements made with this NFA are discussed in the following section.

IV. Frequency Domain Measurements and Lookup Table Assembly

To validate the interrogation antenna design, measurement and simulation in freespace are compared over the 2-20 GHz decade. The resulting complex S_{11} traces are shown in Fig. 6. Once validated, measurements against stacked materials are made. The materials used to build seventeen different stacks are shown in Fig. 7, alongside the interrogation antenna. The properties of each material are given in Table I, including thickness, d_i, as well as dispersive permittivity and conductivity, ϵ_r and σ. The seventeen stack combinations are listed in Table II, where "Layer 1" is the innermost layer.

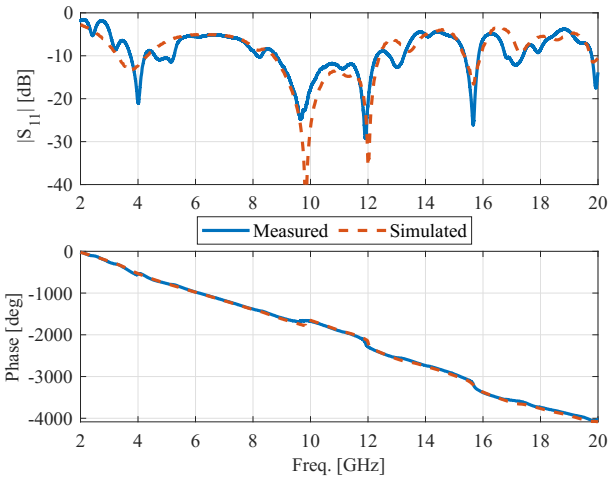

Fig. 6. Simulated and measured complex S_{11} of the interrogation antenna in freespace. The phase is unwrapped and the high values are due to the wide bandwidth of the antenna.

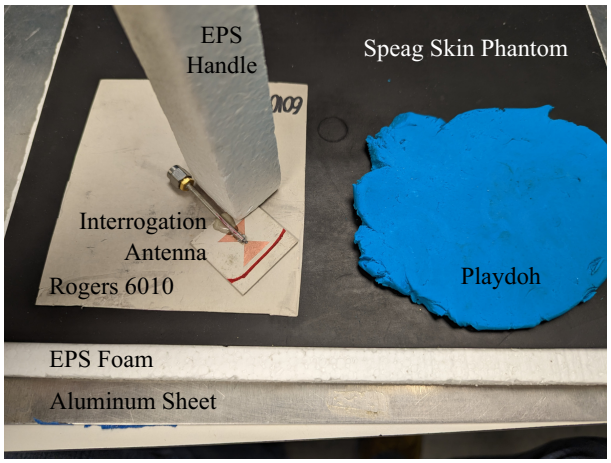

Fig. 7. A photograph of the materials used for the dispersive stack measurements and classifications discussed in this paper. The EPS handle is used to ensure the interrogation antenna is firmly held against the stacks being measured.

TABLE I
Materials Used for Layer Stacks, 2 GHz to 20 GHz

Material	d_i [mm]	ϵ_r	σ [S/m]
EPS Foam	12	1.03	$0.315e^{-15}$
Playdoh	16	30 to 17	5 to 12
Speag Skin	2	28.4 to 21.1	1.03 to 4.1
Rogers 6010	0.635	12.3	$0.4e^{-3}$ to $4.0e^{-3}$

Each of the seventeen stacks is measured using the interrogation antenna four separate times. These four measurements are represented in two ways: as averaged magnitude and absolute value of the frequency-derivative of phase. Features extracted from each averaged representation are added to a lookup table. Then, all 68 measurements are repeated again three times by different people to create three independent trials. Features from these "follow-up" measurements are compared to those in the lookup table to classify the data as corresponding to a particular stack. Actual measurement results for Stack #14 (Al, skin phantom) are shown in Fig. 8

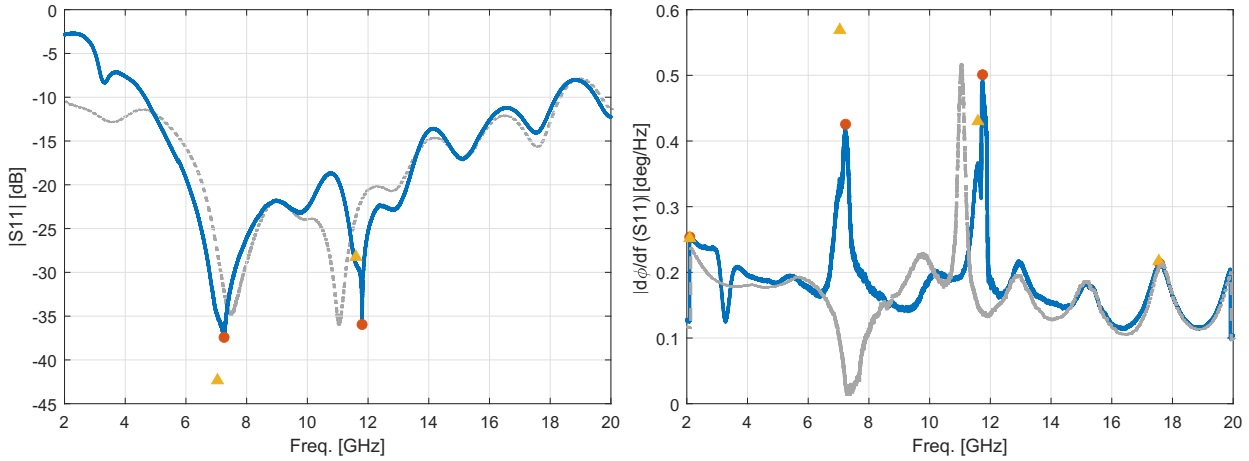

Fig. 8. The magnitude and absolute value of the frequency-derivative of the phase of the S_{11} measurements of Stack #14. The circular features, extracted from the traces shown, are stored in a lookup table. The triangular features are extracted from a follow-up measurement for classification. For comparison, the signatures from Stack #4 are shown in gray.

TABLE II
MEASUREMENT LAYER COMBINATIONS

Stack Num.	Layer 1	Layer 2	Layer 3	Layer 4
1	Al	Playdoh	-	-
2	Al	Playdoh	Rogers 6010	-
3	Al	Playdoh	Rogers 6010	Skin
4	Al	Playdoh	Skin	-
5	Al	Rogers 6010	-	-
6	Al	Rogers 6010	EPS	-
7	Al	Rogers 6010	EPS	Skin
8	Al	Rogers 6010	Skin	-
9	Al	EPS	-	-
10	Al	EPS	Rogers 6010	-
11	Al	EPS	Rogers 6010	Skin
12	Al	EPS	Skin	-
13	Al	EPS	Skin	Rogers 6010
14	Al	Skin	-	-
15	Al	Skin	Rogers 6010	-
16	Al	Skin	EPS	-
17	Al	Skin	EPS	Rogers 6010

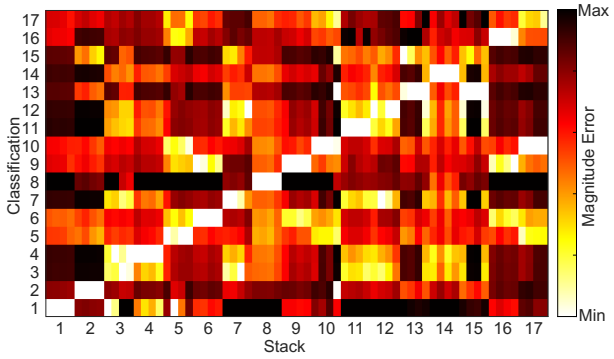

Fig. 9. The resulting error distances, plotted on a log scale, for $|S_{11}|$ features from the first trial. Lighter values indicate smaller errors, and the diagonal represents correctly classified stacks. Each column is normalized to the maximum value in that column. Note that for each number on the x-axis, there are four columns, representing each independent measurement of that stack.

as an illustrative example. Here, the $|S_{11}|$ and the $|\frac{\mathrm{d}}{\mathrm{d}f}\angle S_{11}|$ used to build the lookup table are plotted. The circular markers indicate the features extracted for inclusion in the lookup table while the triangular markers correspond to features extracted from one of the follow-up measurements of the same stack.

V. STACK CLASSIFICATION VIA LOOKUP TABLE

The followup measurements mentioned in the previous section are classified against the lookup table using an error metric. This is repeated for each measurement from each of three different trials. This error metric, a scaled Euclidean distance, is computed as

$$e_1 = \frac{1}{N}\sum_{n=1}^{N}\sqrt{(x_{m,n}-x_{LT,n})^2+\alpha(y_{m,n}-y_{LT,n})^2}, \quad (5)$$

where x_m and y_m are the frequency and magnitude, respectively, for each extracted measurement feature (in dB for $|S_{11}|$ and $\frac{\mathrm{deg}}{\mathrm{Hz}}$ for $|\frac{\mathrm{d}}{\mathrm{d}f}\angle S_{11}|$). Similarly, x_{LT} and y_{LT} are the frequency and magnitude for each feature in the lookup table. α, which is between 0 and 1, is used to de-emphasize the impact of magnitude differences and was empirically set to 0.002 for the measurements. All three are summations of the error metric computed for all features compared and are normalized by the number of features, N, to avoid penalizing feature-rich datasets. The threshold is iteratively adjusted until the measurement and lookup table feature sets contain the same number of features. Results for all three trials are given in Table III.

Data for one trial set of measurements are shown in Fig. 9. The x-axis represents the stack being measured, while the y-axis is each possible stack classification. For each number on the x-axis, there are four columns, corresponding to each individual measurement, for a total of 68 measurements. Each column is normalized to the maximum error in that column and the values are on a log scale to enhance dynamic range. Lighter values represent lower computed error values and correct classifications are along the diagonal.

VI. DISCUSSION AND CONCLUSIONS

In addition to the error metric, e_1, two alternative metrics were considered. The first alternative error metric is an average

TABLE III
RAW STACK CLASSIFICATION ERROR RATES

Operator	Error Metric	Err. Rate	Mag. Err. Rate	dϕ/df Err. Rate
1	e_1	47.1%	41.2%	60.3%
1	e_2	48.5%	47.1%	57.4%
1	e_3	47.1%	48.5%	55.9%
2	e_1	33.8%	29.4%	54.4%
2	e_2	33.8%	30.9%	54.4%
2	e_3	35.3%	30.9%	54.4%
3	e_1	27.9%	27.9%	41.2%
3	e_2	23.5%	26.5%	41.2%
3	e_3	23.5%	26.5%	41.2%

relative distance:

$$e_2 = \frac{2}{N}\sum_{n=1}^{N}\frac{x_{m,n} - x_{LT,n}}{x_{m,n} + x_{LT,n}}, \tag{6}$$

which places equal emphasis on the features in the lookup table and the measurement. Lastly, a fractional relative distance is computed as

$$e_3 = \frac{1}{N}\sum_{n=1}^{N}\frac{x_{m,n} - x_{LT,n}}{x_{LT,n}}, \tag{7}$$

which emphasizes the validity of the lookup table over the measurement. Overall, e_1 performs the best.

As Fig. 9 and Table III illustrate, an error rate of about 35% is average. However, there are several layer combinations that are commonly swapped. These include Stacks 3&4, 6&9, 7&12, 10&17, and 13&15. As evident in Table II, these stacks differ in only a single layer, which might be low-loss or deeply buried. For instance, three of these five stack pairs differ only in the presence (or absence) of the 0.635 mm thick Rogers 6010 layer, which is roughly two orders of magnitude *less* lossy than fat, which is the least lossy actual tissue layer. Thus, while the Rogers 6010 material works well to characterize the limits of this approach, it is not representative of a layer that would appear during *in vivo* measurements. If these swapped stacks are *not* considered strictly misclassified, than the error rate for averaged measurements drops to 6%. In fact, if the follow-up measurements are not averaged (e.g., in Fig. 9), then the error rates fall to 13.2%, 14.7%, and 14.2% for error metrics #1, #2, and #3, respectively.

While this preliminary effort does not directly result in knowledge of properties of stacked media, it does illustrate the viability of the approach for stack composition classification. There are inter-operator variabilities as well as feature extraction issues that can be mitigated in further work. For instance, sparse feature sets, which might include a feature at only one or two frequency locations, can actually lead to artificially invisible layers, if that layer is $\lambda/2$ thick at that frequency. This could be fixed by splitting the 2 GHz to 20 GHz decade into frequency bins and forcing extraction of at least one feature in each bin. Further future work may involve use of advanced non-linear regression schemes for not only classification, but determination of salient layer properties, as done for ultrasound measurements in [14].

VII. ACKNOWLEDGMENTS

Dielectric properties of Playdoh were provided by Dr. Milica Popović, McGill Univ., Montreal, Canada.

REFERENCES

[1] A. Shahzad, S. Khan, M. Jones, R. M. Dwyer, and M. O'Halloran, "Investigation of the effect of dehydration on tissue dielectric properties in ex vivo measurements," *Biomedical Physics & Engineering Express*, vol. 3, no. 4, p. 045001, jun 2017. [Online]. Available: https://dx.doi.org/10.1088/2057-1976/aa74c4

[2] C. Rossmann and D. Haemmerich, "Review of temperature dependence of thermal properties, dielectric properties, and perfusion of biological tissues at hyperthermic and ablation temperatures," *Critical Reviews in Biomedical Engineering*, vol. 42, no. 6, pp. 467–492, 2014.

[3] R. Streeter, G. S. Botello, K. Hall, and Z. Popovic, "Correlation radiometry for subcutaneous temperature measurements," *IEEE Journal of Electromagnetics, RF and Microwaves in Medicine and Biology*, vol. 6, no. 2, pp. 230–237, Jun. 2022.

[4] J. Lee, G. Botello, R. Streeter, K. Hall, and Z. Popovic, "A hybrid correlation-dicke radiometer for internal body thermometry," in *2022 52th European Microwave Conference (EuMC)*, 2022.

[5] J. Hanna, M. Bteich, Y. Tawk, A. H. Ramadan, B. Dia, F. A. Asadallah, A. Eid, R. Kanj, J. Costantine, and A. A. Eid, "Noninvasive, wearable, and tunable electromagnetic multisensing system for continuous glucose monitoring, mimicking vasculature anatomy," *Science Advances*, vol. 6, no. 24, p. eaba5320, 2020.

[6] C. Gabriel, E. H. Grant, and I. R. Young, "Use of time domain spectroscopy for measuring dielectric properties with a coaxial probe," *Journal of Physics E: Scientific Instruments*, vol. 19, no. 10, pp. 843–846, oct 1986. [Online]. Available: https://doi.org/10.1088/0022-3735/19/10/016

[7] D. Popovic, L. McCartney, C. Beasley, M. Lazebnik, M. Okoniewski, S. Hagness, and J. Booske, "Precision open-ended coaxial probes for in vivo and ex vivo dielectric spectroscopy of biological tissues at microwave frequencies," *IEEE Transactions on Microwave Theory and Techniques*, vol. 53, no. 5, pp. 1713–1722, 2005.

[8] H. Zhang, S. Y. Tan, and H. S. Tan, "An improved method for microwave nondestructive dielectric measurement of layered media," *Progress In Electromagnetics Research B*, vol. 10, pp. 145–161, 2008.

[9] T. Rovensky, A. Pietrikova, I. Vehec, and M. Kmec, "Measuring of dielectric properties by microstrip resonators in the ghz frequency," in *2015 38th International Spring Seminar on Electronics Technology (ISSE)*, 2015, pp. 192–196.

[10] R. Streeter, G. S. Botello, J. Lee, and Z. Popović, "Near-field thermal radiation reception spatial sensitivity mapping at 1.4 ghz," in *2022 Joint International Biomedical Sciences Instrumentation and Rocky Mountain Bioengineering Symposium (IBSIS-RMBS)*, 2022.

[11] K. Tisdale, A. Bringer, and A. Kiourti, "A core body temperature retrieval method for microwave radiometry when tissue permittivity is unknown," *IEEE Journal of Electromagnetics, RF and Microwaves in Medicine and Biology*, pp. 1–7, 2022.

[12] C. S. Pant, *Atlas of Breast Imaging*, 2nd ed. Jp Medical Ltd, 2012.

[13] S. Gabriel, R. W. Lau, and C. Gabriel, "The dielectric properties of biological tissues: Iii. parametric models for the dielectric spectrum of tissues," *Physics in Medicine & Biology*, vol. 41, no. 11, p. 2271, nov 1996. [Online]. Available: https://dx.doi.org/10.1088/0031-9155/41/11/003

[14] F. Q. Jin, A. E. Knight, A. R. Cardones, K. R. Nightingale, and M. L. Palmeri, "Semi-automated weak annotation for deep neural network skin thickness measurement," *Ultrasonic Imaging*, vol. 43, no. 4, pp. 167–174, 2021, pMID: 33971769. [Online]. Available: https://doi.org/10.1177/01617346211014138

Rob Streeter received B.S. degrees in Electrical as well as Computer Engineering from the University of Wyoming in 2011, a M.S. in Electrical Engineering from the same school in 2013, and a Ph.D in EE from the University of Colorado at Boulder in 2023. He has worked on UAS decision-making algorithms and test protocols for the U.S. Air Force Academy as a Research Engineer; LMR and IP system design, deployment, and maintenance for public and private entities with Ryan Electronics, Inc.; in 2017/18 was a winter-over Research Associate at the Amundsen-Scott South Pole Station (under employment by Leidos for the Antarctic Support Contract, which is operated by the NSF); and currently divides his time as a Site Supervisor for Polar Field Services and a consulting engineer with LumenAstra. Rob's interests are in leadership, engineering education, and interdisciplinary applications of electrical engineering principles.

Gabriel Santamaria received his Electrical Engineering degree from the University of Carabobo, Venezuela in 2014 after completing his final project on the development of a full-wave electromagnetic solver based on the multi-level fast multipole method (MLFMM). In 2015 he joined the Group of Radiofrequency, Electromagnetism, Microwaves, and Antennas at Charles III University of Madrid (UC3M) and obtained his Ph.D. degree in Jan 2021. His Ph.D. thesis mainly focused on the theoretical analysis of THz-to-optical upconversion via resonant electro-optics techniques for high sensitivity THz radiometry. He is currently working on RF field sensing techniques using Rydberg atoms and the development of non-invasive radiometers for internal body temperature measurements.

Jooeun Lee received her B.S. degree in electronics engineering from Pusan National University, Korea, in 2019. Then she earned her M.S. degree in Electrical Engineering from Korea Advanced Institute of Science and Technology (KAIST), Korea, in 2021 with a thesis on CMOS wideband PA and LNA design. She joined the RF and Electromagnetics Group at CU Boulder in fall 2021, where she is pursuing the Ph.D. degree. Her current research is on the development of non-invasive internal body temperature sensors.

Zoya Popović (S'86–M'90–SM'99–F'02) is a Distinguished Professor and the Lockheed Martin Endowed Chair in Electrical Engineering at the University of Colorado, Boulder. She obtained her Dipl.Ing. degree at the University of Belgrade, Serbia, and her Ph.D. at Caltech. She was a Visiting Professor with the Technical University of Munich in 2001/03, ISAE in Toulouse, France in 2014, and was a Chair of Excellence at Carlos III University in Madrid in 2018/19. She has graduated over 65 PhDs and currently advises 17 doctoral students. Her research interests are in high-efficiency power amplifiers and transmitters, microwave and millimeter-wave high-performance circuits for communications and radar, medical applications of microwaves, quantum sensing and metrology, and wireless powering. She is a Fellow of the IEEE and the recipient of two IEEE MTT Microwave Prizes for best journal papers, the White House NSF Presidential Faculty Fellow award, the URSI Issac Koga Gold Medal, the ASEE/HP Terman Medal and the German Alexander von Humboldt Research Award. She was elected as foreign member of the Serbian Academy of Sciences and Arts in 2006. She was named IEEE MTT Distinguished Educator in 2013 and the University of Colorado Distinguished Research Lecturer in 2015.